THE JOURNAL OF PHYSICAL CHEMISTRY B

 VOLUME 106, NUMBER 30, AUGUST 1, 2002

FEATURE ARTICLE

Dramatic Cooperative Effects in Adsorption of NO_x on MgO(001)

William F. Schneider* and Kenneth C. Hass

Ford Research Laboratory, MD 3083/SRL, Dearborn, Michigan 48121-2053

Marina Miletic and John L. Gland

Department of Chemical Engineering, University of Michigan, Ann Arbor, Michigan 48109

Received: March 11, 2002; In Final Form: May 13, 2002

The chemisorption of molecules on metal oxide surfaces is generally considered to occur by either an acid/base or a redox mechanism, with the former dominating on nonreducible and insulating oxides such as MgO. NO, NO_2, and the less familiar NO_3 are atypical adsorbates in that their most potent Lewis acidic and basic forms are generated by one-electron oxidation or reduction of the parent molecules. In this work, first-principles density functional theory supercell calculations are used to probe the adsorption chemistry of the nitrogen oxides on an undefected MgO(001) surface. The isolated adsorbates are found to physisorb (NO, NO_2) or weakly chemisorb (NO_3) to the MgO terrace. In contrast, adsorbate partners located on neighboring surface acid (Mg_s) and base (O_s) sites form strongly chemisorbed products with features characteristic of nitrite (NO_2^-) and nitrate (NO_3^-). The origin of this new class of "cooperative" chemisorption is shown to be electron transfer between two NO_x species to generate Lewis acid (NO_x^+) and base (NO_x^-) pairs that strongly chemisorb to the MgO surface and that are further stabilized by lateral electrostatic attraction. The relatively low ionization potentials and large electron affinities of the NO_x molecules are key to enabling the cooperative effect on MgO. Even more pronounced cooperative effects are expected for NO_x adsorption on more basic or acidic oxides, including those used for NO_x remediation. The effect is also likely to have a role in the heterogeneous chemistry of other odd-electron adsorbates, including the halogen oxides and HO_x radicals.

Introduction

Chemisorption of gaseous species on metal oxide surfaces is of fundamental importance to heterogeneous atmospheric chemistry, environmental catalysis, corrosion, and many other areas of technological significance. The mechanism of interaction of common adsorbates with a metal oxide surface can be divided into two classes: Lewis acid/base—or electron-pair sharing—processes, and oxidation/reduction—or one-electron transfer—processes.[1] The former are characteristic of adsorbates with readily accessible donor or acceptor states. For example, the Lewis acid SO_2 readily accepts a pair of electrons from an anionic site of the basic oxide MgO to form a surface sulfite (SO_3^{2-}):[2−6]

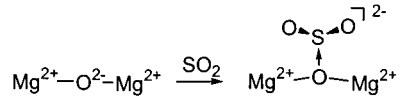

(1)

On the surface of an acidic oxide like α-Al_2O_3, H_2O can both

* To whom correspondence should be addressed. E-mail: wschnei2@ford.com.

10.1021/jp0257496 CCC: $22.00
Published on Web 07/09/2002

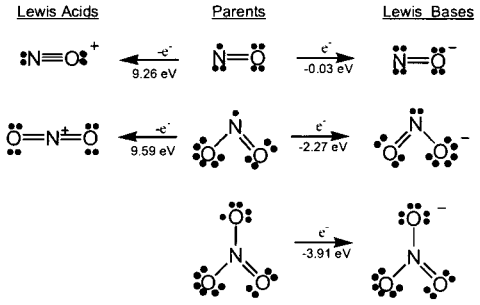

Figure 1. Oxidation and reduction reactions leading to Lewis acidic and basic forms of NO, NO_2, and NO_3. Experimental gas-phase ionization potentials and electron affinities from refs 22 and 23.

adsorb as a simple Lewis base and dissociate into OH^- and H^+ fragments, each of which can combine with the surface as part of a Lewis acid/base pair:[7−10]

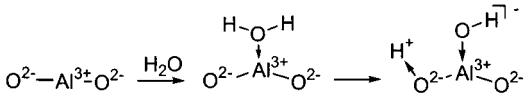

(2)

Oxidation/reduction adsorption processes are typically reserved for semiconducting metal oxides and are associated with changes in cation oxidation state or formation or destruction of oxygen vacancies or both. On strongly insulating and nonreducible metal oxides such as MgO or α-Al_2O_3, redox adsorption is expected to be limited to local defects, if it occurs at all.

The adsorption of nitrogen oxides on metal oxides has particular relevance for environmental chemistry, given the necessity to control the emissions of NO_x ($x = 1, 2$) from stationary and mobile sources.[11,12] For instance, the ability of base metal oxides to adsorb NO_x under oxidizing conditions and to release NO_x under reducing conditions underpins the lean NO_x trap—a leading strategy for lean-burn emissions control.[13] NO, NO_2, and the less common NO_3 are somewhat unusual adsorbates in that they are odd-electron and, while "acidic" in the sense that they hydrolyze to form proton donors, they do not behave as classic Lewis acids. Rather, one-electron oxidation or reduction generates their common Lewis acidic (NO^+ and NO_2^+) and Lewis basic (NO^-, NO_2^-, NO_3^-) forms, respectively (Figure 1). One might expect, then, that the nitrogen oxides would chemisorb on metal oxides via a redox mechanism only and that chemisorption would be limited to surface defects on an insulating metal oxide like MgO. In the case of NO, the available evidence supports this view: NO is known to weakly physisorb on undefected MgO(001)[14−17] but to form more complicated, chemisorbed structures at (001) steps, kinks, and vacancies.[15,18] NO_2, however, is known to chemisorb even on the undefected (001) terraces of MgO to form a mixture of surface nitrite (NO_2^-) and surface nitrate (NO_3^-) species, as identified by their characteristic N near-edge spectra,[14,19,20] with N coverage approaching 0.5 ML.[14] While computation and experiment are in agreement with the weak physisorption of NO on MgO(001),[14,17,21] the ready formation of surface nitrite and nitrate are not completely consistent with the computed adsorption structures and energetics of a single NO_2 molecule on MgO(001),[14,19] and the origins of this NO_2 chemisorption and the nature of the resulting nitrites and nitrates remain to be fully explained.

The oxidation and reduction processes illustrated in Figure 1 suggest a possible alternative, "cooperative" model for NO_x chemisorption on MgO. In this model, transfer of an electron from one NO_x adsorbate to another generates Lewis acid (NO_x^+) and base (NO_x^-) pairs, each member of which can chemisorb in a regular acid/base sense to the metal oxide surface. For a pair of NO_2 adsorbates, for instance, such a process could be conceptually represented as follows:

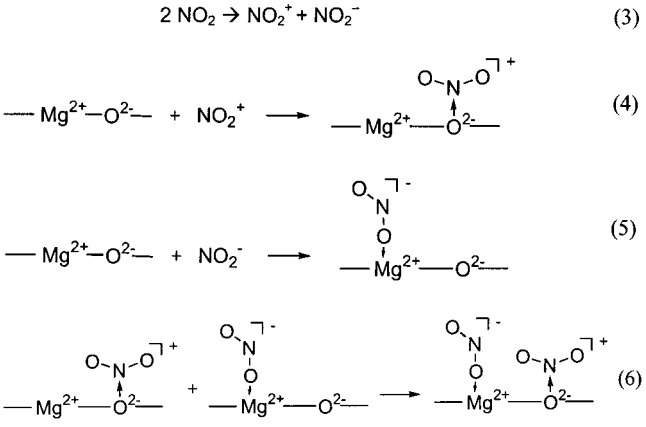

where "−Mg−O−" represents a discrete adsorption site on an ideal (001) surface and the last step involves bringing two remote charged adsorbates into proximity. NO, NO_2, and NO_3 have both relatively low ionization potentials (IP < 10 eV) and large electron affinities (absolute EA > 2.2 eV for NO_2 and NO_3) compared to other adsorbates of potential interest, such as CO_2 (13.8 eV IP and no electron affinity) or SO_2 (12.3 eV IP and 1.1 eV EA).[22,23] Nonetheless, the energy penalty associated with the charge separation in reaction 3 is quite large (7.32 eV for NO_2, Figure 1). For this cooperative mechanism to operate, then, requires a substantial enhancement in the binding of the ionic adsorbate forms over the neutral NO_x species (reactions 4 and 5), as well as a favorable lateral interaction between the oppositely charged centers that result (reaction 6). First-principles calculations on MgO clusters indicate that reactions 4 and 5 are more exothermic than their neutral counterparts,[24] but whether this binding enhancement and the lateral interactions are sufficient to overcome the initial charge separation penalty remains to be explored.

In this work, we use periodic supercell density functional theory (DFT)[25,26] calculations to examine the adsorption of NO_x molecules and coadsorption of NO_x pairs on the undefected (001) terrace of MgO. We demonstrate the existence of a large cooperative adsorption effect that accounts for the observed NO_x chemisorption on MgO and other oxides and that, more importantly, illustrates a new class of chemisorption on metal oxides—one which is neither strictly of the acid/base nor of the oxidation/reduction types but rather is a hybrid of the two.

Computational Details

Periodic supercell, plane wave DFT calculations were performed using the VASP code.[27] The interaction of valence electrons with the atomic core states of Mg, O, and N ions was represented with ultrasoft pseudopotentials,[28] and plane wave basis functions were included to a kinetic energy cutoff of 396 eV. Electronic energies and forces were calculated within the spin-polarized generalized gradient approximation (GGA) using the PW91 functional.[29,30] Appreciable band gaps exist between occupied and virtual states in all of the structures

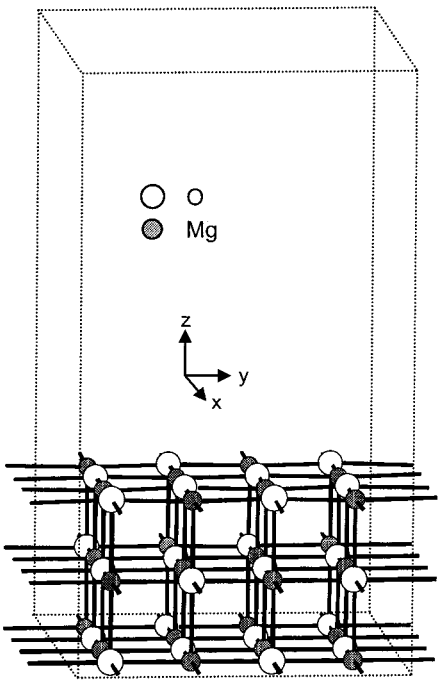

Figure 2. Relaxed MgO(001) 2 × 2 surface model. Supercell dimensions are 8.536 Å × 8.536 Å × 17.072 Å.

considered. Adsorption energies were calculated using the expressions

one NO_x adsorbate

$$\Delta E_{ads} = E^{tot}_{NO_x+slab} - (E^{tot}_{slab} + E^{tot}_{NO_x}) \quad (7)$$

two NO_x adsorbates

$$\Delta E_{ads} = E^{tot}_{NO_x1+NO_x2+slab} - (E^{tot}_{slab} + E^{tot}_{NO_x1} + E^{tot}_{NO_x2}) \quad (8)$$

By this convention $\Delta E_{ads} < 0$ for exothermic adsorption.

Within these approximations, bulk MgO has a lattice constant of 4.268 Å, 1.4% greater than the experimental value of 4.211 Å.[31] The MgO(001) surface is represented with a slab model similar to that described previously.[3] The tetragonal supercell contains 24 MgO formula units arranged in three layers of 16 ions each (we refer to this as the 2 × 2 surface model, Figure 2). The in-plane repeat distance is based on the calculated MgO bulk lattice constant, and the repeat distance in the *c* direction is 17.0 Å, corresponding to a vacuum spacing between unrelaxed slabs of 12.7 Å. A 2 × 2 × 1 Monkhorst−Pack mesh is used to sample the first Brillouin zone; the adsorption results differ only slightly from a Γ-point-only sampling and are converged with respect to denser samplings. In all of the slab calculations, the bottommost layer of ions is fixed at the bulk locations and the remaining ionic positions are relaxed using gradient-based optimization until the residual forces were <0.05 eV/Å. As shown in Figure 2, the (001) surface exhibits only a very slight corrugation in the topmost layer of ions.[32,33] Test calculations with thicker slabs exhibited only slight quantitative differences in the observed adsorbate structures and energetics that do not affect the conclusions of this study.

To explore the distance dependence of lateral adsorbate interactions, some calculations were performed with a 108 atom tetragonal supercell containing three layers of 18 MgO formula units each (labeled the 3 × 3 surface model). The vacuum spacing is comparable to the 2 × 2 model, and again the bottommost layer of ions is frozen in the bulk location in all relaxations. The larger lateral cell dimensions allow Γ-point-only sampling with negligible errors.

To assess qualitative changes in electronic charge distributions upon adsorption, local-orbital supercell calculations were performed using the DMol code.[34,35] Relaxed geometries were taken directly from the plane-wave calculations, and the electronic structure converged within a double numerical plus polarization basis set and Γ-point-only sampling. Charges and spin densities were partitioned among atoms using a standard Mulliken population analysis.

Results and Discussion

NO_x Molecular Adsorption on MgO(001). We begin by considering the adsorption behavior of isolated NO_x molecules at low coverage. Calculations were performed at a variety of coverages using both the 2 × 2 and 3 × 3 surface models. The geometries and binding energies are essentially converged with respect to decreasing coverage at a single NO_x molecule per 2 × 2 cell, and we present those results below.

Gas-phase NO has an experimental bond length of 1.151 Å, and as expected within the GGA, the calculated bond length is slightly (0.021 Å or 1.8%) greater. Previous cluster[15,21,24] and supercell[14,16] calculations are in agreement that isolated NO weakly physisorbs on the undefected (001) terraces of MgO. We examined a variety of N-down and O-down orientations over both acidic Mg_s and basic O_s surface sites. As shown in Figure 3a, in its lowest-energy configuration, NO sits N-down and bent, 2.27 Å above an O_s ion. Adsorption only slightly increases the N−O bond length, and from the Mulliken population analysis (Table 1), charge transfer between the adsorbate and surface is minimal. The calculated adsorption energy of −7.2 kcal mol^{-1} is in good agreement with the experimentally determined low-coverage value of −5.1 kcal mol^{-1}.[17] N-down adsorption at a Mg_s site is higher in energy by approximately 2 kcal mol^{-1}, while O-down adsorption appears to be insignificant. Thus, the very low Lewis acidity and basicity of NO is reflected in its weak physisorption on MgO(001).

Gas-phase NO_2 has a bent structure with an experimental N−O bond length of 1.197 Å and O−N−O bond angle of 134.3°. Again as expected, the GGA slightly overestimates the N−O separation (1.216 Å) and reproduces the bond angle very well (134.2°). A discrete NO_2 molecule can interact with the MgO(001) surface in a variety of conformations,[14,19,24] including O-down and N-down orientations on top or bridging Mg_s and O_s ions. The most energetically preferred O-down and N-down configurations obtained here are also shown in Figure 3, and the corresponding adsorption energies and Mulliken charges are shown in Table 1. Similar to NO, the NO_2 molecule sits >2.2 Å above the (001) surface and is only slightly perturbed from its gas-phase geometry. In the O-down orientation (Figure 3b), NO_2 prefers to bridge two Mg_s ions along the [110] diagonal. In this configuration, NO_2 has an adsorption energy of −10 kcal mol^{-1}; O-down adsorption atop a single Mg_s ion or bridging two ions along the [100] direction[14,19] is found here to be energetically less favorable by >5 kcal mol^{-1}. In the N-down configuration (Figure 3c), NO_2 prefers to sit tilted (N pyramidalized) atop a single O_s ion and in this configuration has an adsorption energy of −4 kcal mol^{-1}. The larger electron affinity and stronger surface binding of NO_2 than NO is reflected in the Mulliken populations by both more appreciable charge transfer from the MgO surface to NO_2 and delocalization of the NO_2 electron "hole" into the MgO surface. These geometry, energetic, and charge distribution results are all consistent with

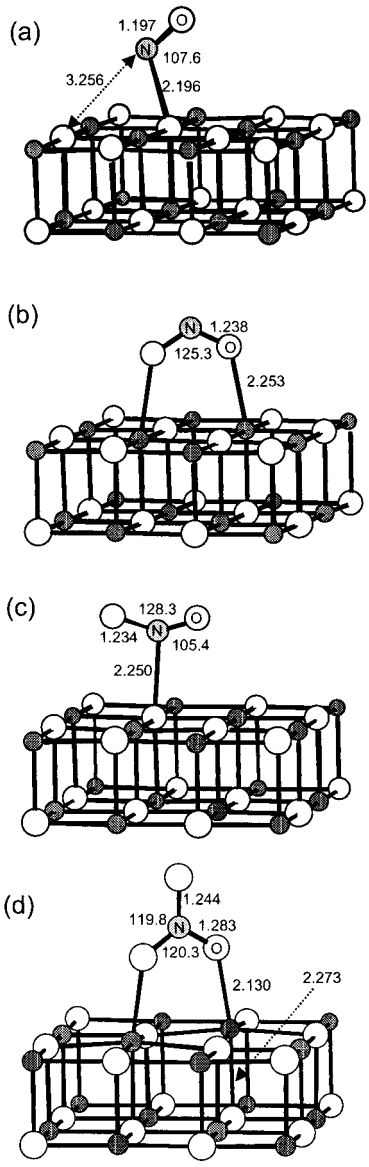

Figure 3. Minimum energy geometries for a single (a) NO, (b) O-down and (c) N-down NO_2, and (d) NO_3 on MgO(001). For clarity, the bottom-most layer of ions is hidden. Distances are given in Å and angles in deg.

a picture of molecular physisorption of NO_2 at low coverages on MgO(001).

In the energetically preferred O-down configuration a single NO_2 adsorbate occupies two Mg_s sites, yielding an effective coverage of $^1/_4$ ML for a single NO_2 on the 2×2 surface model (Figure 3b). This physisorption geometry and energy are remarkably insensitive to surface coverage. The $^1/_4$ ML result is essentially identical to that obtained for $^1/_9$ ML coverage using a 3×3 surface model. At $^1/_2$ ML, constructed from two N-down NO_2 on the 2×2 surface model, the average absolute NO_2 adsorption energy decreases by only a fraction of a kcal mol^{-1}, and even at 1 ML, the adsorption energy is essentially unchanged from the low-coverage limit. When restricted to the O-down adsorption geometry, then, NO_2 is calculated to physisorb on MgO(001) at all coverages.

While molecular NO_3 is an unlikely gas-phase intermediate in environmental NO_x adsorption processes, adsorbed NO_3 is a possible end-point of NO_x adsorption, and thus, it is conceptually useful to consider NO_3 as an adsorbate. Gas-phase NO_3 is trigonal planar with a calculated N−O bond length of 1.254 Å.

TABLE 1: GGA Adsorption Energies (kcal mol^{-1}), Mulliken Gross Charges, and Spin Densities for NO_x Adsorbates on the 2×2 Surface Model, with One Molecule (Top Half of Table) or Pair (Bottom) Per Supercell

	ΔE_{ads}	NO_x charge	NO_x spin density
Molecular Adsorbates			
NO	−7.2	−0.19	0.99
NO_2, O-down	−10.5	−0.26	0.62
NO_2, N-down	−4.3	−0.23	0.78
NO_3	−26.6	−0.72	0.12
Cooperative Adsorbates			
$NO_2^a + NO_2^b$	−30.0	-0.78^a	
		-0.73^b	
$NO^a + NO_2^b$	−33.7	-0.74^a	
		-0.72^b	
$NO_2^a + NO_3^b$	−56.2	-0.78^a	
		-0.79^b	
$NO + NO^c$	−14.8	-0.09^d	
		-0.10^e	

[a] "Acidic" (N-down) NO_x on O_s. Gross charge includes contribution of O_s. [b] "Basic" (O-down) NO_x. [c] Physisorbed NO dimer. [d] O-top NO. [e] Mg-top NO.

Like NO_2, an isolated NO_3 prefers to adsorb perpendicular to the surface and bridging two Mg_s ions along a [110] diagonal (Figure 3d; again alignment along the [100] direction is considerably less-favored). The NO_3 adsorption energy at $^1/_4$ ML is −27 kcal mol^{-1} (Table 1), 2.5 times that of NO_2 and large enough to provide a plausible explanation for the strongly bound surface nitrates observed on NO_2^- exposed MgO, as previously suggested.[19] The origins of this large binding energy enhancement over NO_2 lie in the very high electron affinity of NO_3 and its consequent ability to partially oxidize the MgO surface. Comparison of the Mulliken charges and spin densities of adsorbed NO_2 and NO_3 (Table 1) shows that the latter is much more effective in extracting charge from (and transferring an electron hole to) MgO than is NO_2. The approximately NO_3^--like adsorbate binds strongly to the positive charge induced at the surface. This greater binding is reflected in the 0.10 Å closer approach of an isolated NO_3 than NO or NO_2 to the MgO surface, an increased rumpling of the surface below the adsorbate, and perturbations from the gas-phase geometry that destroy the equivalence of the three N−O bonds.

The pronounced charge polarization induced by NO_3 at the MgO surface suggests that lateral interactions between NO_3 will be much more destabilizing than found above for NO_2. When the same coverage convention is used as that above for NO_2, the adsorption energy per NO_3 at $^1/_9$ ML (3×3 supercell) is −28 kcal mol^{-1}, or just slightly greater than that at $^1/_4$ ML, and decreases to −23 and −19 kcal mol^{-1} at $^1/_2$ and 1 ML, respectively. From these average integral energies, we can estimate the differential adsorption energies at coverages between $^1/_9$ and $^1/_4$, $^1/_4$ and $^1/_2$, and $^1/_2$ and 1 ML to be −26, −19, and −14 kcal mol^{-1}, respectively, so that the binding of a NO_3 to a nearly covered surface is approximately half as strong as that at very low coverage. This marked decrease with coverage reflects increasingly unfavorable electrostatic interactions between NO_3 adsorbates.

NO_x Cooperative Chemisorption on MgO(001). The adsorption phenomena described above involve discrete NO_x molecules interacting with an oxide surface essentially independently (save the unfavorable lateral interactions just discussed) in a single adsorption geometry. As proposed in the Introduction, we now explore the possibility of a cooperative effect between suitably oriented neighboring NO_x within a single 2×2 surface cell.

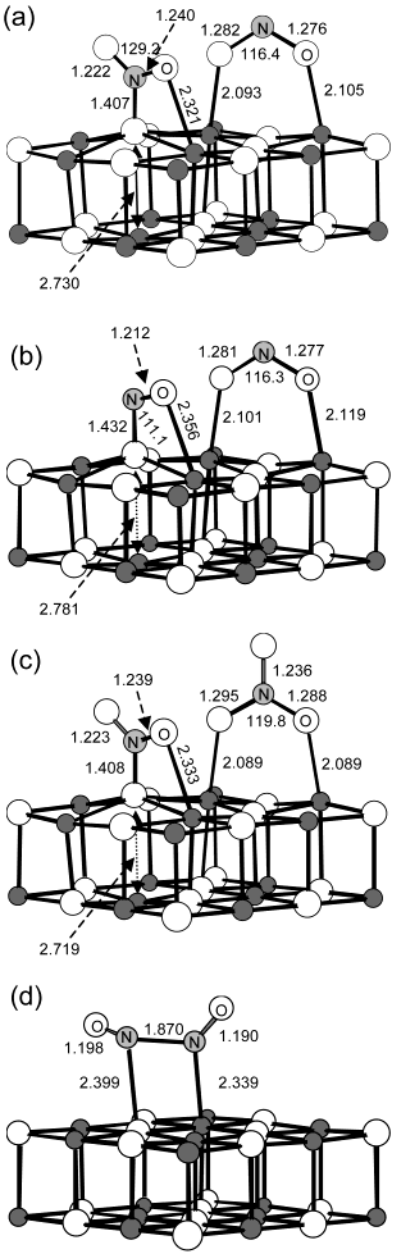

Figure 4. Cooperative chemisorption structures of (a) two NO_2, (b) NO and NO_2, and (c) NO_2 and NO_3, and of (d) the physisorbed NO dimer. For clarity, the bottom-most layer of ions is hidden. Distances are given in Å and angles in deg.

In an initial set of calculations, two NO_2 molecules are placed O-down and N-down in their isolated physisorbed geometries above neighboring Mg_s and O_s ions, respectively, and the system is allowed to relax. The converged geometry for this mixed system shows a dramatic structural and electronic rearrangement indicative of a conversion from physi- to chemisorption (Figure 4a). The basic (O-down on Mg_s) NO_2 relaxes toward the surface and the underlying Mg_s are drawn up such that the adsorbate NO_2-Mg_s separation decreases by 0.14 Å, while the O−N−O angle closes from 125° to 117°. The acidic (N-down on O_s) NO_2 exhibits an even greater relaxation into the surface; coupled with the large upward movement of the underlying O_s, the O_s-NO_2 separation is decreased by >0.8 Å from its physisorbed value, clearly reflecting the formation of a much stronger surface−adsorbate bond. The N center flattens such that the O_s-NO_2 forms an approximately trigonal planar unit, which tilts along the [100] direction to bind bidentate to an adjacent Mg_s. These structural changes are consistent with the model suggested in eqs 3−6 and with the results of cluster calculations on positively and negatively charged NO_2 adsorbates:[24] specifically, that electron transfer between two adjacent NO_2 converts them into a strongly adsorbing Lewis basic NO_2^- anion, or surface nitrite, and Lewis acidic NO_2^+ cation, the latter combining with a surface O^{2-} anion to form an NO_3^-, or surface nitrate (Figure 4a). We can represent this net process as follows:

$$MgO(001) + 2NO_2 \rightarrow [MgO](NO_2^+)(NO_2^-) \qquad (9)$$

The energy penalty associated with this charge transfer is more than compensated for in enhanced surface bonding: the combined absolute adsorption energy of a NO_2 pair as represented by reaction 9 is 15 kcal mol^{-1} greater than that of isolated O-down and N-down NO_2 individually, or nearly twice as great (Table 1). This enhancement in surface bonding of adjacent adsorbates is an example of the *cooperative bonding effect*, which provides a mechanism for chemisorption of NO_2 on MgO(001).

Charge analysis supports this charge-transfer model. The adsorbate-localized unpaired electrons of isolated physisorbed NO_2 are absent in the cooperative system, and a large energy gap opens between the occupied and virtual states. The gross charge on the basic NO_2 increases by almost 0.5 e^-, while that on the acidic NO_2 decreases by an equivalent amount. The net charges on the basic NO_2 and acidic NO_2 plus O_s fragments become nearly equal (Table 1) and are consistent with the qualitative descriptions NO_2^- and NO_3^-, respectively. Thus, in the absence of further surface reaction, NO_2 cooperative chemisorption yields a surface that can be characterized as mixed nitrite and nitrate. The formation of a mixture of nitrite and nitrate has been observed on NO_2-exposed MgO surfaces, although not in the 1:1 ratio that reaction 9 would suggest.[19] As described more fully in the Discussion section below, disproportionation and further oxidation of the cooperatively adsorbed NO_2 can account for the observed excess nitrate.

This cooperative bonding effect is not restricted to adjacent adsorption sites, and in fact, the effect appears to fall off rather slowly with lateral separation of the acidic and basic NO_2. Because the acidic site is locally depleted in charge and the basic site enhanced, the two are electrostatically attracted to one another, as suggested by reaction 6. We have used the 3×3 surface model to explore the presence and magnitude of the cooperative effect as a function of separation of the two adsorbate sites. Assuming the basic NO_2 to adsorb O-down bridging two nearest-neighbor Mg_s cations, as above, six symmetry-unique O_s sites can be identified for adsorption of the acidic NO_2 in the 3×3 model (Figure 5a). (The nonuniqueness of the remaining O_s sites is readily evident from the local C_{2v} symmetry about the occupied Mg_s sites.) These six are labeled O_a-O_f in Figure 5a, ordered by distance from the Mg_s-Mg_s centroid to the occupied O_s site. Geometry relaxations were performed for adsorbate pairs at all possible separations. In all cases, the local adsorbate geometries (adsorbate−surface bond distances and angles) are remarkably similar to that shown in Figure 4a and reflect the presence of a cooperative bonding effect. The most notable geometric differences occur with adsorption at site O_a, nearest neighbor to the two occupied Mg_s sites, where steric interactions cause the planar NO_2^- and NO_3^- anions to orient parallel (along [110]) but tilted away from one another. These repulsive

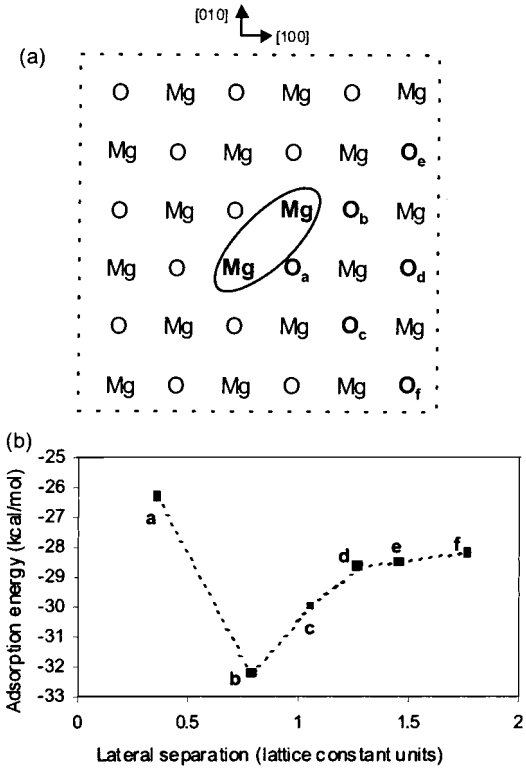

Figure 5. Top view (a) of 3 × 3 surface model showing location of basic NO_2 adsorption site (circled) and six corresponding symmetry-unique acidic NO_2 adsorption sites (O_a−O_f) and (b) total adsorption energy as function of adsorbate separation.

interactions dominate over the electrostatic attraction effect, and this adsorption site is the least stable of the ones considered (Figure 5b).

At all of the remaining adsorption sites (O_b−O_f), two different rotational conformations of the forming NO_3^- anion are possible, corresponding to orientation along one of the two perpendicular ([100] and [010]) ion rows. At site O_b, sterics dictate a strong preference for orientation in the direction in which both neighboring Mg_s sites are vacant ([010] in Figure 5a). The combination of minimal steric repulsion and near maximal electrostatic attraction makes this the preferred location for the acidic NO_2 (Figure 5b). This is the site illustrated in Figure 4a for the 2 × 2 surface model, and the structure and energetics are nearly identical in the 3 × 3 model. The slight (2 kcal mol^{-1}) increase in total binding of the cooperatively adsorbed NO_2 pair at this site in the 3 × 3 model over the 2 × 2 may reflect a decrease in long-range interactions between adsorbate pairs in neighboring cells, but the magnitude of the effect is too small to draw definitive conclusions. At sites O_c and beyond, the two possible acidic NO_2 orientations become essentially equivalent sterically, and the gradual decrease in total binding shown in Figure 5b reflects the decreasing electrostatic attraction between the acidic and basic sites. At the greatest separations possible with the 3 × 3 model, interactions between oppositely charged adsorbates in neighboring cells begin to contribute to the overall binding, so that the total binding energy begins to level off. At site O_f, cooperative effects still produce an adsorption energy 15 kcal mol^{-1} greater than an infinitely separated physisorbed NO_2 pair.

Most significant from these results is the observation that the cooperative bonding effect can operate well beyond nearest neighbor cation and anion adsorption sites. The magnitude of the electronic coupling between acidic and basic NO_2 can be further probed by reversing the spin of the unpaired electron on one of the two adsorbates, thus artificially blocking the electron transfer underlying the cooperative effect. Regardless of lateral separation, in this triplet-constrained state unpaired electrons remain localized on the two adsorbates and the system relaxes to two physisorbed NO_2 with total adsorption energy equal to the sum of two isolated adsorbates. Electron transfer between adsorbates is essential to the operation of the cooperative bonding effect.

This cooperative bonding mechanism could, in principle, operate for any combination of Lewis acid and base in Figure 1. For instance, the combination of NO^+ as acid and NO_2^- as base can be achieved by placing a NO N-down on an O_s and a NO_2 O-down on Mg_s. The relaxed geometry of such a pair within the 2 × 2 surface model is shown in Figure 4b. As with the NO_2 pair discussed above, the NO and NO_2 relax from their isolated physisorbed geometries in a fashion that reflects cooperative chemisorption. The basic NO_2 is drawn toward the underlying Mg_s ions and the O−N−O angle is narrowed such that the final adsorbate geometry is nearly identical to that discussed above for the Lewis basic half of the NO_2 cooperative pair. Again, the relaxation associated with the acidic species is even more pronounced and is consistent with cluster model results:[24] the O_s ion is drawn out of the surface and the NO pulled in such that the O_s−NO distance decreases by 0.76 Å from its physisorbed value, and the NO rotates so that the terminal O atom can coordinate with a nearest neighbor Mg_s. The overall reaction

$$\mathrm{MgO(001)} + \mathrm{NO} + \mathrm{NO_2} \rightarrow \mathrm{[MgO](NO^+)(NO_2^-)} \quad (10)$$

is exothermic by −32 kcal mol^{-1}, or more than twice that of adsorption of the isolated physisorbed species, again reflecting the operation of a strong cooperative effect.

The NO and NO_2 pair thus provides a model for a nitrited MgO surface. Consistent with cluster calculations,[24] two distinct types of surface nitrite (NO_2^-) are identified, the first generated by one-electron reduction of NO_2 and the second by one-electron oxidation of O_s^{2-} + NO. The former retains the C_{2v} symmetry of a classic nitrite ion, while the latter is distorted by its asymmetrical coordination to the surface. As shown in Table 1, the two formed nitrite anions have nearly identical gross Mulliken charges of magnitude consistent with a monoanion description. The distribution of charge among the atoms does differ, and combined with the geometric distinctions just noted, we would expect two spectroscopically distinct types of surface nitrite to be distinguishable. To our knowledge such distinctions have not yet been observed on MgO, although vibrational spectroscopy has been interpreted in terms of multiple nitrite types on NO_x-exposed alumina and baria.[36]

A cooperative model for a nitrated surface can similarly be constructed by choosing NO_2^+ as acid and NO_3^- as base in Figure 1, that is, by placing NO_2 N-down on an O_s and NO_3 O-down on an adjacent Mg_s. The relaxed structure for this combination is shown in Figure 4c. As noted above, a NO_3 adsorbate is strongly oxidizing and readily forms a surface nitrate (NO_3^-) on MgO. In the isolated NO_3 case, the excess charge is abstracted from the MgO surface, but in the cooperative case, the neighboring O_s^{2-} + NO_2 combination provides a more ready electron source. Thus, the O-down NO_3 fragment adopts a structure quite similar to that observed for isolated NO_3 (Figure 3d), with the somewhat closer approach to the underlying Mg_s cations and slightly greater local accumulation of negative charge (Table 1) reflecting the relative ease of electron transfer. The NO_2 on O_s^{2-} donates one electron to form a nitrate with structure essentially identical to that observed for the nitrate

partner of the $NO_2 + NO_2$ cooperative pair (Figure 4a). As with the nitrite surface then, two structurally distinct types of surface nitrate are possible, one bound to acidic Mg_s and the other to basic O_s.[24] The NO_2 and NO_3 cooperative pair

$$MgO(001) + NO_2 + NO_3 \rightarrow [MgO](NO_2^+)(NO_3^-) \quad (11)$$

has an adsorption energy of -56 kcal mol^{-1} (Table 1), significantly exceeding that of isolated NO_2 and NO_3 molecular adsorbates. It is interesting to note that further oxidation of this cooperative nitrate by NO_2 to the molecularly adsorbed NO_3 species is highly disfavored ($\Delta H_{calc} = 37$ kcal mol^{-1} in the 2×2 model and at constant N coverage):

$$[MgO](NO_2^+)(NO_3^-) + NO_2 \rightarrow 2[MgO](NO_3) + NO \quad (12)$$

providing further support for the cooperative model for surface nitrate.

Not all combinations of acid and base from Table 1 necessarily produce a cooperatively bound pair on MgO(001). For instance, the most stable conformation of a pair of NO on MgO(001) is shown in Figure 4d. While the NO prefer to sit above neighboring Mg_s and O_s, they do not chemisorb as NO^+ and NO^-. Rather, the large separation from the surface and relatively close N−N approach indicate formation of a physisorbed NO dimer, and these dimers dominate NO physisorption on MgO.[15,21] The slight increase in net adsorption energy relative to two isolated NO (Table 1) is a consequence of the dimer bond formation rather than any enhanced adsorption effect. Mulliken analysis does show a small but uniform charge transfer from MgO to the dimer constituents, which is known to contribute to the shortening and strengthening of the ON−NO bond.[37] We consider the factors influencing the presence or absence of the cooperative bonding effect below.

Discussion

Nitrites and Nitrates on MgO(001). Room-temperature exposure of MgO(001) to NO_2 has been reported on the basis of X-ray spectroscopic analyses to produce a mixture of surface nitrite and nitrate, with the latter in severalfold excess.[14,19] Thermal annealing of this mixture initially depletes the nitrite feature and ultimately removes the nitrate as well. While the high NO_2 exposures used in these experiments likely produce surface coverages greater than those considered in this work, we can propose some qualitative interpretations based on the cooperative bonding model results. The initial chemisorbed species expected upon MgO(001) exposure to NO_2 is the cooperative bound NO_2, which includes an equal proportion of surface nitrite and nitrate (reaction 9). An excess of nitrate can be created by the further oxidation of some of the surface nitrite by NO_2:[19]

$$[MgO](NO_2^+)(NO_2^-) + NO_2 \rightarrow [MgO](NO_2^+)(NO_3^-) + NO \quad (13)$$

At the coverages considered here, reaction 13 is essentially thermoneutral ($\Delta H_{calc} = 1$ kcal mol^{-1} in the 2×2 surface model). Further oxidation of the cooperative pair to two [MgO]-NO_3 (reaction 12) is strongly endothermic so that the latter surface species cannot be produced in isolation on MgO from exposure to NO_2. The mix of surface species can also be altered via disproportionation reactions:

$$2[MgO](NO_2^+)(NO_2^-) \rightarrow [MgO](NO_2^+)(NO_3^-) + [MgO](NO^+)(NO_2^-) \quad (14)$$

Reaction 14 is slightly exothermic ($\Delta H_{calc} = -3$ kcal mol^{-1} within the 2×2 model). The actual fraction and types of nitrite and nitrate will thus depend on the chemical potentials of NO and NO_2, temperature, and the details of lateral interaction and kinetic effects; clearly, however, the cooperative model is consistent with a varied and unequal mix of surface nitrite and nitrate.

The preferential thermal loss of nitrite from this complex surface can then be understood in terms of the energetics of destruction of cooperative pairs. Loss of a nitrite cooperative pair,

$$[MgO](NO^+)(NO_2^-) \rightarrow [MgO](NO_2) + NO \quad (15)$$

or of a mixed nitrite−nitrate pair,

$$[MgO](NO_2^+)(NO_2^-) \rightarrow [MgO](NO_2) + NO_2 \quad (16)$$

requires 23 and 20 kcal mol^{-1}, respectively, at the coverages considered here and likely less at higher coverages. The isolated NO_2 remaining is bound by at most 10 kcal mol^{-1} and, unless it finds another partner, will readily desorb at the temperatures required to destroy the cooperative pair. In contrast, loss of a nitrate pair,

$$[MgO](NO_2^+)(NO_3^-) \rightarrow [MgO](NO_3) + NO_2 \quad (17)$$

costs 30 kcal mol^{-1}, or approximately 50% more energy than the nitrite-containing ones, and leaves behind a nitrite-like NO_3 with appreciable surface binding energy. From these comparisons, then, a surface containing a mixture of nitrite and nitrate is expected to evolve by initial depletion of nitrite and, only at higher temperatures, by loss of nitrate, as observed.[19] Temperature-programmed desorption experiments at varying coverages would be useful for clarifying this chemistry and further substantiating the cooperative model.

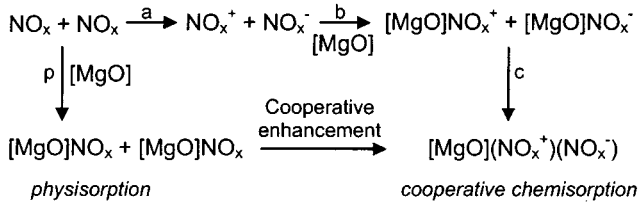

Figure 6. Thermodynamic cycle for the cooperative bonding effect.

Chemical Basis for the Cooperative Bonding Effect. The charge transfer, adsorption, and lateral interaction contributions to cooperative bonding can be conveniently analyzed in terms of the thermodynamic cycle shown in Figure 6; Table 2 contains the corresponding energy details for the NO_x adsorbates considered here. Starting from the upper left corner of the figure and moving clockwise, the first step (a) in the cycle is formation of the gas-phase ions from the neutrals; the energy of this charge separation step is simply the difference between the ionization potential (IP) of the first and electron affinity (EA) of the second species, which for the NO_x molecules are readily available from experiment (Figure 1). These differences are all positive but strongly dependent on the chemical identities of the constituents. In the second step (b), the two ions are separately adsorbed on

TABLE 2: Thermodynamic Cycle Energies (kcal mol^{-1}) from the 2 × 2 Surface Model[a]

		cooperative chemisorption				
acid/base	physisorption (p)	a	b[b]	c	a + b + c	cooperative enhancement
NO_2/NO_2 (mixed)	−14.8	168.7	−143.9	−54.8	−30.1	−15.2 (103%)
NO/NO_2 (nitrite)	−17.7	161.1	−145.8	−49.0	−33.7	−15.6 (90%)
NO_2/NO_3 (nitrate)	−30.8	130.1	−133.9	−53.2	−56.2	−25.3 (82%)
NO/NO	−14.4	212.7	−140.3	∼−50[c]	∼+22	

[a] Refer to Figure 6 for the description of individual steps. [b] From ref 24. [c] Estimated by comparison with cooperative adsorbates.

isolated acidic and basic surface sites. The energies of these processes are unavailable from experiment or supercell calculations, but reasonable estimates can be obtained from MgO cluster calculations.[24] Adsorption of the cation to MgO is always much stronger than the anion because of the basicity of MgO, but as shown in Table 2, the sum of the two adsorption energies is nearly constant across all partners, ranging from 70 kcal mol^{-1} less than (for NO^+ and NO^-) to slightly greater than (for NO_2^+ and NO_3^-) the charge separation energy (a). As previously noted, the adsorption energies of the ions are also much larger than those of the neutrals (step p in the figure and table), reflecting the much greater Lewis acidity and basicity of the ions over the neutrals.[24] In the third step (c), the two charged adsorbates are brought together on neighboring surface sites. Because this quantity is difficult to obtain directly, we estimate it by difference, subtracting a + b from the cooperative chemisorption sum (a + b + c) available from the supercell results here. Because the electrostatics underlying step c are similar for all of the adsorbates, this term is nearly constant.

A cooperative effect thus requires that the cooperative sum be greater than the physisorption energy (step p). For NO/NO_2, NO_2/NO_2, and NO_2/NO_3 this condition is met: the greater chemisorption energy of the ions nearly compensates for the cost of charge separation, and the electrostatic attraction of the charged adsorbates more than makes up the remaining difference. From this analysis, it also becomes clear why the effect does not operate for the NO/NO pair. Because a cooperative adsorbate does not exist in this case, we assume the energy of step c to be similar to that of the other pairs, or about −50 kcal mol^{-1}, and calculate the cooperative sum directly. The large charge separation energy (a) in this case overwhelms the other two terms so that the sum not only does not exceed the physisorption value, but it is not even negative. The charge separation energy is thus seen to be the key element in determining the existence and magnitude of the cooperative bonding effect for NO_x on MgO.

This model underscores the importance of charge transfer to the cooperative bonding model. Clearly, this charge transfer is not spontaneous in the gas-phase and must be facilitated by the interaction of adsorbates with the oxide surface. The results in Figure 5 indicate that transfer between physisorbed NO_2 is favorable over several angstroms of separation. However, the actual dynamics of electron transfer, including the relative contributions of through-space and surface-mediated transfer, remain to be explored.

While their small IPs and large EAs may make the higher nitrogen oxides particularly well-suited to this chemistry, they are almost certainly not unique in their ability to form cooperative adsorbates on metal oxides. Another likely example, the halogen oxides, including ClO_x, BrO_x, and IO_x, $x = 1-4$, are also odd-electron molecules that readily oxidize to Lewis acids and reduce to Lewis bases. For instance, the differences between the IP and EA of ClO, BrO, and IO radical are approximately 200, 185, and 170 kcal mol^{-1},[22,23] respectively, comparable to the range of NO_x values. While little data are available, the higher halogen oxides are expected to have even smaller charge-separation costs. Assuming that the halogen ions have Lewis acidity and basicity similar to the NO_x ions, then, one would expect similar cooperative bonding effects to influence halogen oxide chemisorption. HO and HO_2 radicals also are potentially Lewis amphiphilic; the charge separation penalties for them are 259 and 237 kcal mol^{-1},[22,23] respectively, likely too large to effect chemisorption on MgO bonding but potentially of importance on materials of greater Lewis acidity and basicity. The heterogeneous chemistries of halogen oxides and HO_x radicals, along with the nitrogen oxides, are relevant to atmospheric processes including stratospheric ozone depletion and tropospheric smog formation; these results suggest that cooperative effects may play a previously unrecognized role in this chemistry.

Another key element of cooperative bonding is the availability of proximal Lewis acid and base adsorption sites on the surface of interest. The MgO(001) surface does not present particularly strongly acidic or basic sites, and thus, it is likely that other oxides will evidence an even more dramatic cooperative effect. Experimental results for NO_x adsorption on BaO—a much more basic oxide than MgO—provide strong evidence for the formation and thermal loss of mixed nitrites and nitrates consistent with a cooperative bonding mechanism.[38] A recent DFT study of NO_2 chemisorption on BaO(001) implies a cooperative effect much larger than that found here for MgO.[39] More acidic oxides, such as alumina or the transition metal oxides, may show cooperative effects that have a greater contribution from the basic member of the cooperative pair. These effects may even play a role in the NO_x chemistry of zeolites, with their discrete and localized acidic and basic sites. Consideration of these cooperative effects in materials other than MgO is the subject of ongoing investigation.

Conclusions

The computational evidence presented here strongly supports the notion of a third hybrid class of adsorption behavior on oxide surfaces supplementing the normally considered acid/base and redox processes. This cooperative bonding effect results from the enhancement in Lewis acidity and basicity made possible by charge transfer between pairs of adsorbates combined with the lateral electrostatic attraction induced by charge separation. The effect is illustrated for NO_x adsorption on MgO(001): while isolated NO, NO_2, and NO_3 molecularly adsorb on the surface with binding energies ranging from physisorption to relatively low-energy chemisorption, electron transfer between pairs of adsorbates produce strongly chemisorbing ions that provide reasonable representations of the surface nitrites and nitrates observed experimentally. Two types of surface nitrite and nitrate are distinguished, depending on their association with surface acid (Mg_s) or surface base (O_s) sites. A general thermodynamic cycle to describe this phenomenon has been developed (Figure 6), which separates the overall effect into its underlying charge-transfer, adsorption, and electrostatic components. The energy penalty associated with charge transfer is found to be the key

term controlling NO_x cooperative chemisorption on MgO; other terms may dominate with different surfaces or adsorbates. We anticipate this to be the first of many examples of the cooperative bonding effect on amphiphilic oxide surface and believe it to be an important step forward in understanding the NO_x surface chemistry central to numerous environmental and exhaust aftertreatment processes.

Acknowledgment. We thank Pete Schmitz, John Li, Dairene Uy, and Alex Bogicevic of the Ford Research Laboratory for helpful discussions and comments regarding NO_x adsorption on oxides, Ita Panas and Peter Broqvist for generously sharing results prior to publication, and David J. Mann for performing the DMol calculations.

References and Notes

(1) Henrich, V. E.; Cox, P. A. *The Surface Science of Metal Oxides*; Cambridge University Press: Cambridge, U.K., 1994.
(2) Schoonheydt, R. A.; Lunsford, J. H. *J. Catal.* **1972**, *26*, 261.
(3) Schneider, W. F.; Li, J.; Hass, K. C. *J. Phys. Chem. B* **2001**, *105*, 6972.
(4) Rodriguez, J. A.; Jirsak, T.; Freitag, A.; Larese, J. Z.; Maiti, A. *J. Phys. Chem. B* **2000**, *104*, 7439.
(5) Pacchioni, G.; Clotet, A.; Ricart, J. M. *Surf. Sci.* **1994**, *315*, 337.
(6) Pacchioni, G.; Ricart, J. M.; Illas, F. *J. Am. Chem. Soc.* **1994**, *116*, 10152.
(7) Elam, J. W.; Nelson, C. E.; Cameron, M. A.; Tolbert, M. A.; George, S. M. *J. Phys. Chem. B* **1998**, *102*, 7008.
(8) McHale, J. M.; Auroux, A.; Perrotta, A. J.; Navrotsky, A. *Science* **1997**, *277*, 788.
(9) Hass, K. C.; Schneider, W. F.; Curioni, A.; Andreoni, W. *Science* **1998**, *282*, 265.
(10) Hass, K. C.; Schneider, W. F.; Curioni, A.; Andreoni, W. *J. Phys. Chem. B* **2000**, *104*, 5527.
(11) Taylor, K. C. *Catal. Rev.-Sci. Eng.* **1993**, *35*, 457.
(12) Shelef, M.; McCabe, R. W. *Catal. Today* **2000**.
(13) Miyoshi, N.; Matsumoto, S.; Katoh, K.; Tanaka, T.; Harada, J.; Takahashi, N.; Yokota, K.; Sugiura, M.; Kasahara, K. *Soc. Automot. Eng.* **1995**, 19950809.
(14) Rodriguez, J. A.; Jirsak, T.; Kim, J.-Y.; Larese, J. Z.; Maiti, A. *Chem. Phys. Lett.* **2000**, *330*, 475.
(15) Di Valentin, C.; Pacchioni, G.; Chiesa, M.; Giamello, E.; Abbet, S.; Heiz, U. *J. Phys. Chem. B* **2002**, *106*, 1637.
(16) Rodriguez, J. A.; Jirsak, T.; Pérez, M.; González, L.; Maiti, A. *J. Chem. Phys.* **2001**, *114*, 4186.
(17) Wichtendahl, R.; Rodriguez-Rodrigo, M.; Härtel, U.; Kuhlenbeck, H.; Freund, H.-J. *Phys. Status Solidi A* **1999**, *173*, 93.
(18) Platero, E.; Spoto, G.; Zecchina, A. *J. Chem. Soc., Faraday Trans. 1* **1985**, *81*, 1283.
(19) Rodriguez, J. A.; Jirsak, T.; Sambasivan, S.; Fischer, D.; Maiti, A. *J. Chem. Phys.* **2000**, *112*, 9929.
(20) Rodriguez, J. A.; Pérez, M.; Jirsak, T.; González, L.; Maiti, A.; Larese, J. Z. *J. Phys. Chem. B* **2001**, *105*, 5497.
(21) Lu, X.; Xu, X.; Wang, N.; Zhang, Q. *J. Phys. Chem. B* **1999**, *103*, 5657.
(22) Bartmess, J. E. *NIST Chemistry Webbook, NIST Standard Reference Database Number 69*; National Institutes of Standards and Technology: Gaithersburg, MD, 2001.
(23) Lias, S. G. *NIST Chemistry Webbook, NIST Standard Reference Database Number 69*; National Institutes of Standards and Technology: Gaithersburg, MD, 2001.
(24) Miletic, M.; Gland, J. L.; Schneider, W. F.; Hass, K. C. *J. Phys. Chem. B*, submitted for publication.
(25) Parr, R. G.; Yang, W. *Density-Functional Theory of Atoms and Molecules*; Oxford University Press: New York, 1999.
(26) Payne, M. C.; Teter, M. P.; Allan, D. C.; Arias, T. A.; Joannopoulos, J. D. *Rev. Mod. Phys.* **1992**, *64*, 1045.
(27) Kresse, G.; Furthmüller, J. *Comput. Mater. Sci.* **1996**, *6*, 15.
(28) Vanderbilt, D. *Phys. Rev. B* **1990**, *41*, 7892.
(29) Perdew, J. P.; Wang, Y. *Phys. Rev. B* **1992**, *45*, 13244.
(30) Perdew, J. P.; Chevary, J. A.; Vosko, S. H.; Jackson, K. A.; Pederson, M. R.; Singh, D. J.; Fiolhais, C. *Phys. Rev. B* **1992**, *46*, 6671.
(31) Wycoff, R. W. G. *Crystal Structures*; Interscience: New York, 1963.
(32) Langel, W.; Parrinello, M. *J. Chem. Phys.* **1995**, *103*, 3240.
(33) Kantorovich, L. N.; Holender, J. M.; Gillan, M. J. *Surf. Sci.* **1995**, *343*, 221.
(34) Delley, B. *J. Chem. Phys.* **1990**, *92*, 508.
(35) Baker, J.; Kessi, A.; Delley, B. *J. Chem. Phys.* **1996**, *105*, 192.
(36) Westerberg, B.; Fridell, E. *J. Mol. Catal. A: Chem.* **2001**, *165*, 249.
(37) Ramprasad, R.; Hass, K. C.; Schneider, W. F.; Adams, J. B. *J. Phys. Chem. B* **1997**, *101*, 6903.
(38) Schmitz, P. J.; Baird, R.; Miletic, M.; Gland, J. L. *J. Phys. Chem. B* **2002**, *106*, 4172.
(39) Broqvist, P.; Panas, I.; Fridell, E.; Persson, H. *J. Phys. Chem. B* **2002**, *106*, 137.